Diagn Interv Radiol 2026; DOI: 10.4274/dir.2026.264060

NEURORADIOLOGY

ORIGINAL ARTICLE

Factors associated with early hematoma expansion in intracerebral hemorrhage and the value of non-contrast computed tomography imaging features combined with clinical data for early identification

Jun Ding[1#]
Ying Shao[1#]
ChunHong Meng[2]

[1]The First Affiliated Hospital of Wannan Medical College (Yijishan Hospital of Wannan Medical College), Department of Radiology, Wuhu, China

[2]The First Affiliated Hospital of Wannan Medical College (Yijishan Hospital of Wannan Medical College), Department of Ultrasound Medicine, Wuhu, China

PURPOSE

Early hematoma expansion (HE) after intracerebral hemorrhage (ICH) critically affects patient outcomes. Identifying HE risk using emergency non-contrast computed tomography (NCCT) features and clinical data is important for early risk stratification and evaluation. This study analyzed factors associated with early HE and evaluated the value of NCCT features combined with clinical data for HE identification.

METHODS

A total of 571 patients with spontaneous supratentorial ICH admitted between January 2022 and December 2025 were enrolled. Five NCCT signs were evaluated at baseline. Four signs significantly associated with HE (black hole, swirl, blend, and satellite signs) were summed to construct a primary comprehensive sign score (0–4); a 5-sign score additionally including the island sign was examined in a sensitivity analysis. Patients were stratified by HE status, sign score quantiles, sex, and hematoma morphology, then randomly assigned to training (n = 391) and validation (n = 180) sets. Univariate and multivariate logistic regression identified independent HE factors and constructed a combined prediction model. Model performance was evaluated using receiver operating characteristic curves, calibration curves, and decision curve analysis (DCA). HE was defined as an absolute volume increase > 6 mL or a relative increase > 33% on follow-up CT compared with baseline CT.

RESULTS

Among 571 patients, 292 (51.1%) experienced early HE. Multivariate analysis showed that the 4-sign score [odds ratio (OR): 1.850, 95% confidence interval (CI): 1.505–2.274, $P < 0.001$], irregular hematoma morphology (OR: 2.071, 95% CI: 1.262–3.399, $P = 0.004$), time from onset to initial CT (OR: 0.845, 95% CI: 0.750–0.953, $P = 0.006$), male sex (OR: 1.500, 95% CI: 1.028–2.189, $P = 0.036$), and baseline CT attenuation (OR: 0.964, 95% CI: 0.934–0.995, $P = 0.024$) were independently associated with HE. The primary combined model achieved an area under the curve (AUC) of 0.731 (95% CI: 0.682–0.781) in the training set and 0.716 (95% CI: 0.641–0.791) in the validation set. The 5-sign sensitivity model showed similar discrimination (AUC: 0.722 and 0.704, respectively), with no significant difference ($P = 0.188$ and $P = 0.283$). Calibration and DCA were broadly comparable between models.

CONCLUSION

A 4-sign comprehensive imaging score, irregular hematoma morphology, time from onset to initial CT, male sex, and baseline CT attenuation were independently associated with early HE in patients with ICH.

CLINICAL SIGNIFICANCE

A model based on NCCT features combined with clinical data may provide a practical adjunct for early HE risk stratification in patients with ICH.

KEYWORDS

Intracerebral hemorrhage, hematoma expansion, non-contrast computed tomography, imaging signs, prediction model, associated factors

#Equal contributions to this study.

Handling editor: Erkan Gökçe

Corresponding author: ChunHong Meng

E-mail: MMengch@outlook.com

Received 13 April 2026; revision requested 07 May 2026; last revision requested 09 July 2026; accepted 29 July 2026.

Epub: 05.08.2026

Publication date:

DOI: 10.4274/dir.2026.264060

You may cite this article as: Ding J, Shao Y, CH Meng. Factors associated with early hematoma expansion in intracerebral hemorrhage and the value of non-contrast computed tomography imaging features combined with clinical data for early identification. *Diagn Interv Radiol*. 05 August 2026 DOI: 10.4274/dir.2026.264060 [Epub Ahead of Print].

Spontaneous intracerebral hemorrhage (ICH) is one of the acute stroke subtypes with the highest mortality and disability rates. It has a sudden onset and rapid progression, often leading to neurological deterioration within a short period, and overall outcomes remain poor.[1,2] Despite recent advances in blood pressure management, coagulation reversal, intensive care, and stroke unit management, there remains a lack of sufficiently precise and convenient early risk stratification tools in the acute phase of ICH. Therefore, identifying objective markers for early risk assessment upon admission is of great clinical importance.[3]

Hematoma expansion (HE) is considered one of the most critical adverse events with potential for intervention during the dynamic evolution of acute ICH.[4,5] Previous studies have shown that HE predominantly occurs in the early stage after onset, particularly within the first few hours, and is closely associated with early neurological deterioration, increased mortality, and poor long-term functional outcomes.[6] Currently, HE is commonly defined as an absolute increase in hematoma volume > 6 mL or a relative increase > 33%. This definition demonstrates a stable correlation with patient outcomes and provides a consistent foundation for HE-related research.[7] Therefore, early identification of HE not only facilitates risk assessment but also aids in optimizing clinical decisions regarding repeat imaging, monitoring, and treatment strategies.

Previous research has indicated that clinical factors such as baseline hematoma volume, time from onset to initial imaging, and history of antithrombotic or anticoagulant therapy are associated with HE risk, leading to the development of several clinical prediction tools.[8,9] Concurrently, the value of imaging factors in identifying HE has garnered widespread attention. Although the computed tomography (CT) angiography (CTA) spot sign has high predictive value for HE, the accessibility and applicability of CTA in emergency settings remain limited. Conversely, non-contrast CT (NCCT) is rapid, easy to perform, and widely available, making it the most common initial imaging examination for patients with ICH upon admission. Consequently, early risk identification based on NCCT aligns more closely with clinical practice.[4,10]

Recent accumulating evidence suggests that beyond confirming the location and extent of hemorrhage, NCCT can also reflect hematoma activity through signs such as intraparenchymal hematoma density heterogeneity, irregular margin morphology, and surrounding small foci of bleeding.[11-15] Various NCCT signs, including the hypodensity sign, black hole sign, island sign, satellite sign, and swirl sign, have been reported to be associated with HE, indicating that NCCT provides valuable information for risk stratification. Further studies have shown that combining NCCT imaging features with clinical factors may enhance the ability to predict HE, making predictions more relevant to clinical decision-making.[16]

Based on this, the present study was conducted to analyze factors associated with early HE in patients with ICH by integrating NCCT imaging features with clinical data to further evaluate their predictive value for HE, thereby providing a reference for early risk stratification and clinical management in patients with ICH upon admission.

Main points

- A comprehensive non-contrast computed tomography (NCCT) imaging sign score combining the black hole, swirl, blend, and satellite signs is independently associated with early hematoma expansion (HE) in spontaneous intracerebral hemorrhage (odds ratio: 1.850, $P < 0.001$).
- Irregular hematoma morphology, shorter time from onset to initial CT, male sex, and lower baseline CT attenuation are independent predictors of early HE.
- A prediction model integrating the 4-sign NCCT score with clinical data demonstrates moderate discriminative ability for early HE (area under the curve: 0.731 in the training set and 0.716 in the validation set) and provides net benefit in decision curve analysis.

Methods

Study design and participants

This study consecutively enrolled patients with spontaneous ICH admitted to The First Affiliated Hospital of Wannan Medical College (Yijishan Hospital of Wannan Medical College) between January 2022 and December 2025. Inclusion criteria: aged ≥ 18 years; diagnosis of spontaneous supratentorial ICH confirmed by NCCT of the head; time from onset to initial CT < 6 hours; follow-up CT completed within 24–48 hours after admission; and complete clinical and imaging data. Exclusion criteria: secondary ICH (including definite etiologies, such as vascular malformation, tumor hemorrhage, hemorrhagic cerebral infarction, and trauma); surgical or interventional treatment prior to admission; pregnancy; thrombolytic therapy prior to admission; or poor image quality precluding sign assessment. Prior use of antiplatelet or anticoagulant medications was collected as baseline data and was not considered an exclusion criterion. Informed consent was obtained from all individual participants included in the study. Ethics committee approval was obtained from The First Affiliated Hospital of Wannan Medical College (Yijishan Hospital of Wannan Medical College) (approval number: 2026-43, date: 3 February 2026).

Computed tomography scanning protocol and imaging data acquisition

All patients underwent standard NCCT of the head (slice thickness 5 mm) without contrast enhancement. Two neuroradiologists (J.D. and Y.S.) who had received specialized training independently reviewed the images without knowledge of patient outcomes, and disagreements were resolved by consensus.

Hematoma volume was calculated using the Tada formula: volume (mL) = length (cm) × width (cm) × height (cm) × $\pi/6$. Baseline CT attenuation was measured as the mean CT density (Hounsfield units, HU) within the region of interest at the largest cross-section of the hematoma, reflecting the homogeneity of hematoma density. Hematoma morphology was classified by the reviewing physicians as regular (near-circular or elliptical) or irregular (including lobulated, jagged, and multifocal confluent forms), recorded as a binary variable. Additionally, the presence of intraventricular hemorrhage (IVH) and cerebral herniation was recorded.

Construction of a comprehensive non-contrast computed tomography imaging sign score

For each patient, baseline CT images were evaluated for five imaging signs associated with HE based on standardized definitions from previous literature. The black hole sign was assessed using both morphologic and quantitative criteria and was defined as a well-defined, round or oval hypodense area fully encapsulated within a hyperdense hematoma, with a density difference of ≥ 28 HU between the hypodense area and the surrounding hematoma. The swirl sign was defined as an irregular mixed isodense or hypodense region within a hyperdense hematoma, extending across at least two consecutive axial slices. The blend sign was defined as adjacent regions within the hematoma with a density difference ≥ 18 HU and a clearly discernible boundary. The satellite sign was defined as small hemorrhagic foci adjacent to or mildly separated from the

outer margin of the main hematoma. The island sign was defined as the presence of at least three hemorrhagic foci completely separated from the main hematoma, or at least four hemorrhagic foci partially separated from the main hematoma. Each sign was assigned a score of 1 if present and 0 if absent. Because the island sign was not significantly associated with HE in the present cohort, the primary comprehensive imaging score was constructed as the sum of the black hole, swirl, blend, and satellite signs (range, 0–4). A 5-sign score additionally including the island sign (range, 0–5) was evaluated in a sensitivity analysis.

Clinical data collection

The following baseline clinical data were collected: demographic data, including sex and age; information related to onset, including time from onset to initial CT (hours); admission vital signs, including systolic and diastolic blood pressure; neurological status, assessed using the Glasgow Coma Scale (GCS) score; medical history and medication use, including history of hypertension, regular use of antihypertensive medications, history of diabetes mellitus, regular use of glucose-lowering medications, history of long-term alcohol consumption (defined as alcohol consumption for ≥ 1 year with a frequency of ≥ 2 times per week), history of antiplatelet agent (aspirin) use, and history of warfarin use. All data were entered by uniformly trained researchers and independently verified to ensure data consistency.

Outcome definition

The primary outcome of this study was early HE. According to internationally accepted criteria, HE was defined as an absolute increase in hematoma volume > 6 mL or a relative increase > 33% on follow-up CT compared with baseline CT, with the presence of either criterion considered HE-positive. Hematoma volumes were consistently calculated using the same formula, and follow-up CT was completed within 24–48 hours after admission to minimize the influence of factors other than the natural evolution of the hematoma on outcome determination.

Statistical analysis

All statistical analyses were performed using R software (version 4.4.1). Continuous variables were expressed as mean ± standard deviation or median (interquartile range) according to their distribution, with intergroup comparisons conducted using the t-test or Mann–Whitney U test, as appropriate. Categorical variables were expressed as numbers and percentages, with intergroup comparisons performed using the chi-square test or Fisher's exact test. All patients were randomly assigned to a training set and a validation set using stratified randomization according to HE status, quantiles of the 4-sign comprehensive imaging score, sex, and hematoma morphology. In the training set, univariate and multivariate logistic regression analyses were used to identify factors independently associated with early HE, and a combined prediction model was constructed accordingly. Discrimination was evaluated using receiver operating characteristic curves and areas under the curve (AUCs), calibration was assessed using calibration intercepts, slopes, Brier scores, and calibration curves, and decision curve analysis (DCA) was used to estimate clinical net benefit. As a sensitivity analysis, the 5-sign score, including the island sign, was substituted for the primary 4-sign score while retaining the remaining predictors and the same training–validation split. The two combined models were compared using paired DeLong tests, calibration metrics, and DCA. All tests were two-sided, and a P value of < 0.05 was considered statistically significant.

Results

Baseline characteristics of the study population

A total of 687 patients with ICH were screened during the study period. After excluding 116 patients due to non-compliance with inclusion criteria or missing key data, 571 patients were ultimately included in the analysis (Figure 1). Among these 571 patients, 292 (51.1%) experienced early HE (HE group), and 279 (48.9%) did not (non-HE group). The mean age of the entire cohort was 61.5 ± 12.8 years, and 372 patients (65.1%) were male. A history of hypertension was present in 385 patients (67.4%), diabetes mellitus in 64 patients (11.2%), and a history of alcohol consumption in 92 patients (16.1%) (Table 1).

No statistically significant differences were observed between the two groups in terms of age, history of hypertension, regular use of antihypertensive or glucose-lowering medications, history of alcohol consumption, history of aspirin or warfarin use, diastolic blood pressure, GCS score, or incidence of IVH (all $P > 0.05$). Compared with the non-HE group, the HE group had a significantly higher proportion of male patients (70.2% vs. 59.9%, $P = 0.009$), higher admission systolic blood pressure (170.6 ± 28.8 mmHg vs. 164.9 ± 26.5 mmHg, $P = 0.013$), and shorter time from onset to initial CT (median 3.0 hours vs. 4.0 hours, $P = 0.001$). Additionally, the HE group had a larger baseline hematoma volume (22.6 mL vs. 13.3 mL, $P < 0.001$) and a higher incidence of cerebral herniation (28.2% vs. 18.3%, $P = 0.005$).

Non-contrast computed tomography imaging features and distribution of the four-sign comprehensive imaging score

Among all 571 patients, irregular hematoma morphology was observed in 469 patients (82.1%), with a significantly higher proportion in the HE group than in the non-HE group (87.7% vs. 76.3%, $P < 0.001$). Among the five imaging signs, the blend sign had the highest detection rate (145 patients, 25.4%), followed by the black hole sign (132 patients, 23.1%), satellite sign (80 patients, 14.0%), island sign (77 patients, 13.5%), and swirl sign (89 patients, 15.6%). Except for the island sign ($P = 0.104$), the remaining four signs showed significant differences between the HE and non-HE groups (all $P < 0.001$): the positive rate of the black hole sign was 33.2% in the HE group vs. 12.5% in the non-HE group; the swirl sign was 24.0% vs. 6.8%; the blend sign was 33.9% vs.16.5%; and the satellite sign was 18.8% vs. 9.0% (Table 1, Figure 2).

The distribution of the 4-sign comprehensive imaging score differed significantly between the two groups, with higher scores observed in the HE group ($P < 0.001$). In the non-HE group, 69.2% of patients had a score of 0, compared with 39.4% in the HE group. As the score increased, the proportion of patients in the HE group rose progressively: score 1 (30.1% vs. 22.2%), score 2 (17.8% vs. 4.3%), and score ≥ 3 (12.7% vs. 4.3%), indicating a positive gradient between the cumulative number of imaging signs and HE risk (Table 1, Figure 2).

Logistic Regression Analysis of Independent Predictors of Hematoma Expansion

Univariate logistic regression analysis showed that male sex [odds ratio (OR): 1.580, 95% confidence interval (CI): 1.117–2.235, $P = 0.010$), time from onset to initial CT (OR: 0.835, 95% CI: 0.748–0.932, $P = 0.001$), admission systolic blood pressure (OR: 1.007, 95% CI: 1.001–1.012, $P = 0.028$), baseline CT attenuation (OR: 0.972, 95% CI: 0.944–1.000, $P = 0.050$), baseline hematoma volume (OR: 1.015, 95% CI: 1.007–1.023, $P < 0.001$), irregular hematoma morphology (OR: 2.203, 95% CI: 1.412–3.438, $P < 0.001$), the 4-sign com-

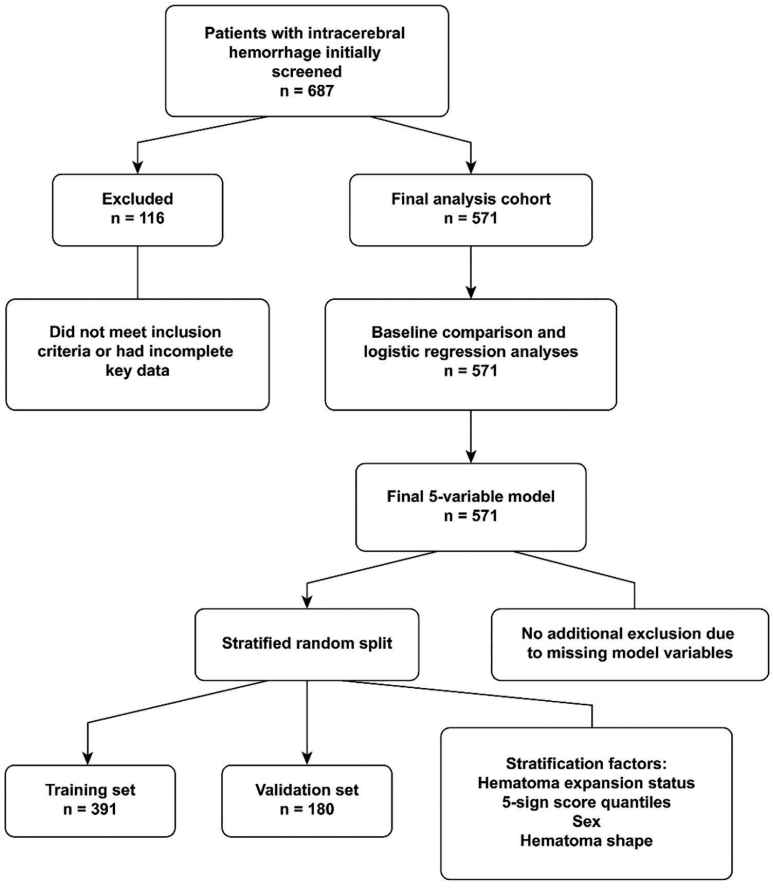

Figure 1. Flowchart of patient enrollment and dataset allocation. Of 687 patients initially screened, 116 were excluded due to failure to meet inclusion criteria or incomplete key data, resulting in a final analytic cohort of 571 patients. The cohort was subsequently divided into a training set (n = 391) and a validation set (n = 180) using stratified random splitting, with stratification by hematoma expansion status, comprehensive imaging sign score, sex, and hematoma morphology.

prehensive imaging score (OR: 1.972, 95% CI: 1.622–2.396, $P < 0.001$), and cerebral herniation (OR: 1.754, 95% CI: 1.180–2.608, $P = 0.006$) were significantly associated with HE. Age, hypertension, diabetes mellitus, admission diastolic blood pressure, GCS score, and IVH were not statistically significant (all $P > 0.05$) (Table 2).

After variables with $P < 0.05$ in univariate analysis were entered into the multivariable logistic regression model, the 4-sign comprehensive imaging score (OR: 1.850, 95% CI: 1.505–2.274, $P < 0.001$), irregular hematoma morphology (OR: 2.071, 95% CI: 1.262–3.399, $P = 0.004$), time from onset to initial CT (OR: 0.845, 95% CI: 0.750–0.953, $P = 0.006$), male sex (OR: 1.500, 95% CI: 1.028–2.189, $P = 0.036$), and baseline CT attenuation (OR: 0.964, 95% CI: 0.934–0.995, $P = 0.024$) remained independently associated with HE. Baseline hematoma volume, admission systolic blood pressure, and cerebral herniation were not statistically significant in the multivariable model (all $P > 0.05$) (Table 2).

Diagnostic performance evaluation of the combined prediction model

A combined prediction model was constructed using the five independent predictors identified above. In the training set (n = 391), the primary 4-sign combined model achieved an AUC of 0.731 (95% CI: 0.682–0.781), with a sensitivity of 56.0%, specificity of 79.6%, and accuracy of 67.5% at the optimal cut-off. The AUC for the 4-sign score alone was 0.679, and the AUCs for the remaining individual predictors ranged from 0.548 to 0.580. In the validation set (n = 180), the primary model achieved an AUC of 0.716 (95% CI: 0.641–0.791), with a sensitivity of 83.7%, specificity of 50.0%, and accuracy of 67.2%. The AUC for the 4-sign score alone was 0.649, and the AUCs for the remaining individual predictors ranged from 0.547 to 0.570 (Table 3, Figure 3).

Calibration analysis showed acceptable agreement between predicted and observed probabilities for the primary 4-sign combined model in both the training and validation sets (Figure 4).

DCA showed that the primary 4-sign combined model provided higher net benefit than the treat-all and treat-none strategies across threshold probabilities of approximately 0.20–0.82 in the training set and 0.23–0.76 in the validation set (Figure 5).

In the sensitivity analysis, the combined 5-sign model including the island sign yielded an AUC of 0.722 (95% CI: 0.672–0.773) in the training set and 0.704 (95% CI: 0.628–0.779) in the validation set. These values did not differ significantly from those of the primary 4-sign model in either the training set ($P = 0.188$) or the validation set ($P = 0.283$) (Figure 3c and d). Calibration was broadly comparable between the models. In the validation set, the calibration intercept and slope were –0.013 and 0.903 for the 4-sign model and 0.017 and 0.992 for the 5-sign model, with similar Brier scores (0.217 and 0.218, respectively) (Figure 4). The two models also showed largely overlapping ranges of net benefit on DCA (Figure 5).

Table 1. Baseline characteristics of patients according to hematoma expansion status

Variable	Overall (n = 571)	Non-HE (n = 279)	HE (n = 292)	*P* value
Demographic and medical history				
Age, years	61.5 ± 12.8	62.0 ± 12.8	61.0 ± 12.7	0.308
Male sex, n (%)	372 (65.1)	167 (59.9)	205 (70.2)	0.009
History of hypertension, n (%)	385 (67.4)	185 (66.3)	200 (68.5)	0.578
Regular antihypertensive therapy, n (%)	226 (39.6)	118 (42.3)	108 (37.0)	0.195
Diabetes mellitus, n (%)	64 (11.2)	31 (11.1)	33 (11.3)	0.943
Regular antidiabetic therapy, n (%)	49 (8.6)	24 (8.6)	25 (8.6)	0.986
Alcohol use history, n (%)	92 (16.1)	50 (17.9)	42 (14.4)	0.250
Prior aspirin use, n (%)	56 (9.8)	25 (9.0)	31 (10.6)	0.506
Prior warfarin use, n (%)	14 (2.5)	6 (2.2)	8 (2.7)	0.649
Admission clinical status				
Systolic blood pressure on admission, mmHg	167.8 ± 27.8	164.9 ± 26.5	170.6 ± 28.8	0.013
Diastolic blood pressure on admission, mmHg	95.9 ± 18.7	94.6 ± 16.8	97.1 ± 20.3	0.105
Glasgow Coma Scale score on admission	13.0 (9.0, 14.0)	13.0 (9.0, 14.0)	13.0 (10.0, 13.0)	0.892
Time from onset to first CT, h	3.5 (2.0, 5.0)	4.0 (2.5, 5.0)	3.0 (2.0, 4.0)	0.001
Baseline CT features				
Intraventricular extension, n (%)	213 (37.4)	96 (34.5)	117 (40.1)	0.172
Herniation, n (%)	133 (23.3)	51 (18.3)	82 (28.2)	0.005
Baseline hematoma volume, mL	18.1 (8.7, 32.0)	13.3 (7.2, 24.8)	22.6 (11.9, 36.2)	< 0.001
Irregular hematoma shape, n (%)	469 (82.1)	213 (76.3)	256 (87.7)	< 0.001
Black hole sign, n (%)	132 (23.1)	35 (12.5)	97 (33.2)	< 0.001
Swirl sign, n (%)	89 (15.6)	19 (6.8)	70 (24.0)	< 0.001
Blend sign, n (%)	145 (25.4)	46 (16.5)	99 (33.9)	< 0.001
Satellite sign, n (%)	80 (14.0)	25 (9.0)	55 (18.8)	< 0.001
Island sign, n (%)	77 (13.5)	31 (11.1)	46 (15.8)	0.104
NCCT sign score (4-sign), n (%)				< 0.001
0	308 (53.9)	193 (69.2)	115 (39.4)	
1	150 (26.3)	62 (22.2)	88 (30.1)	
2	64 (11.2)	12 (4.3)	52 (17.8)	
≥ 3	49 (8.6)	12 (4.3)	37 (12.7)	

Continuous variables are presented as mean ± SD or median (IQR) as appropriate for distribution; categorical variables are presented as n (%); *P* values were calculated using Welch's t-test for approximately normally distributed continuous variables, Mann–Whitney U test for skewed or ordinal variables, and chi-square test or Fisher's exact test for categorical variables, as appropriate. The primary NCCT sign score was constructed as the sum of the black hole, swirl, blend, and satellite signs (each scored 0 or 1) and is presented categorically as 0, 1, 2, and ≥ 3. CT, computed tomography; HE, hematoma expansion; NCCT, non-contrast computed tomography; IQR, interquartile range; SD, standard deviation.

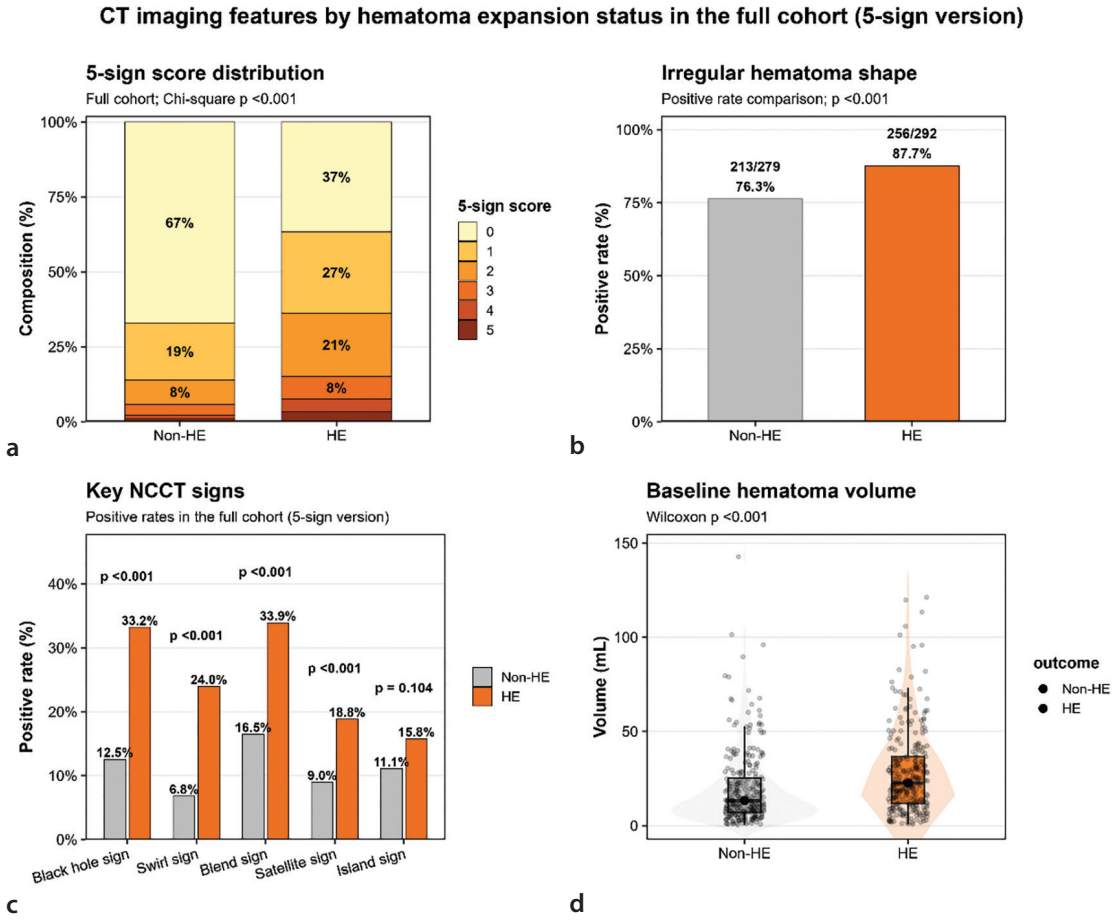

Figure 2. Distribution of NCCT imaging features in the full cohort stratified by HE status. The figure shows (**a**) the primary 4-sign score distribution, (**b**) irregular hematoma morphology, (**c**) positive rates of individual NCCT signs, and (**d**) baseline hematoma volume according to hematoma expansion status. Bar charts show the prevalence of each CT imaging feature among patients with HE and those without HE. The primary 4-sign comprehensive imaging score is presented categorically as 0, 1, 2, and ≥ 3 positive signs; *P* values were derived from chi-square tests. CT, computed tomography; NCCT, non-contrast CT; HE, hematoma expansion.

Table 2. Univariable and multivariable logistic regression analyses for predictors of hematoma expansion

Variable	Comparison	Univariable OR (95% CI)	Univariable *P*	Multivariable OR (95% CI)	Multivariable *P*
Age, years	Per 1-year increase	1.001 (0.995–1.007)	0.689	—	—
Male sex	Male vs. female	1.580 (1.117–2.235)	0.010	1.500 (1.028–2.189)	0.036
Time from onset to first CT, h	Per 1-hour increase	0.835 (0.748–0.932)	0.001	0.845 (0.750–0.953)	0.006
Hypertension	Yes vs. no	1.105 (0.778–1.568)	0.578	—	—
Diabetes	Yes vs. no	1.019 (0.606–1.715)	0.943	—	—
SBP at admission, mmHg	Per 1-mmHg increase	1.007 (1.001–1.012)	0.028	1.004 (0.998–1.011)	0.210
DBP at admission, mmHg	Per 1-mmHg increase	1.006 (0.998–1.015)	0.158	—	—
GCS score	Per 1-point increase	1.010 (0.948–1.076)	0.754	—	—
Baseline CT attenuation, HU	Per 1-HU increase	0.972 (0.944–1.000)	0.050	0.964 (0.934–0.995)	0.024
Baseline hematoma volume, mL	Per 1-mL increase	1.015 (1.007–1.023)	< 0.001	1.006 (0.997–1.014)	0.185
Irregular hematoma shape	Irregular vs. regular	2.203 (1.412–3.438)	< 0.001	2.071 (1.262–3.399)	0.004
NCCT sign score (4-sign)	Per 1-point increase	1.972 (1.622–2.396)	< 0.001	1.850 (1.505–2.274)	< 0.001
Intraventricular hemorrhage	Yes vs. no	1.267 (0.902–1.782)	0.172	—	—
Herniation	Yes vs. no	1.754 (1.180–2.608)	0.006	1.320 (0.848–2.055)	0.219

Results are expressed as ORs with 95% CIs. Variables with $P < 0.05$ in univariable analysis were simultaneously entered into the multivariable logistic regression model. Variables not reaching $P < 0.05$ in univariable analysis were not entered and are indicated by "—". The primary NCCT sign score (4-sign) was analyzed as a continuous variable per 1-point increase. HU, Hounsfield units; CT, computed tomography; GCS, Glasgow Coma Scale; SBP, systolic blood pressure; DBP, diastolic blood pressure; OR, odds ratio; CI, confidence interval.

Table 3. Discrimination performance of the primary 4-sign model, the 5-sign sensitivity model, and individual predictors in the training and validation sets

Model	AUC (95% CI)	Cut-off	Sensitivity	Specificity	Accuracy
Training set					
Combined 4-sign	0.731 (0.682–0.781)	0.549	0.560	0.796	0.675
Combined 5-sign	0.722 (0.672–0.773)	0.517	0.630	0.754	0.691
sign_score4	0.679 (0.632–0.727)	0.500	0.610	0.702	0.655
baseline_ct_hu	0.548 (0.491–0.605)	64.050	0.460	0.634	0.545
first_ct_time_h	0.580 (0.524–0.636)	4.250	0.765	0.382	0.578
shape_irregular	0.558 (0.520–0.595)	0.500	0.885	0.230	0.565
sex_male	0.554 (0.507–0.601)	0.500	0.705	0.403	0.558
Validation set					
Combined 4-sign	0.716 (0.641–0.791)	0.411	0.837	0.500	0.672
Combined 5-sign	0.704 (0.628–0.779)	0.427	0.793	0.523	0.661
sign_score4	0.649 (0.576–0.722)	0.500	0.598	0.670	0.633
baseline_ct_hu	0.570 (0.485–0.654)	65.500	0.609	0.580	0.594
first_ct_time_h	0.569 (0.487–0.652)	4.250	0.793	0.352	0.578
shape_irregular	0.554 (0.496–0.612)	0.500	0.859	0.250	0.561
sex_male	0.547 (0.477–0.617)	0.500	0.696	0.398	0.550

Sensitivity, specificity, and accuracy correspond to the optimal cut-off determined by the Youden index in each dataset. For baseline CT attenuation and time to first CT, lower values indicate higher predicted risk, and ROC analysis was performed accordingly. The primary combined model included the 4-sign NCCT score, irregular hematoma shape, time from onset to first CT, male sex, and baseline CT attenuation. The 5-sign sensitivity model additionally included the island sign in the composite score. Paired DeLong tests showed no significant difference between the models in the training set ($P = 0.188$) or validation set ($P = 0.283$). ROC, receiver operating characteristic; AUC, area under the curve; CI, confidence interval; CT, computed tomography; NCCT, non-contrast CT.

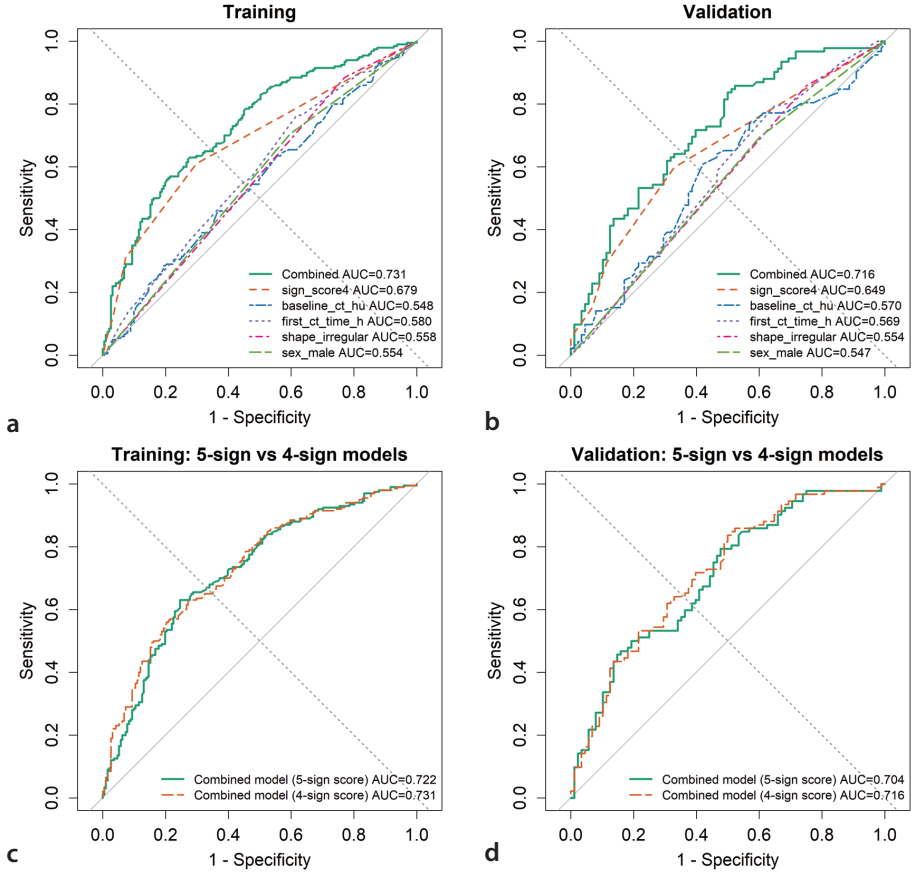

Figure 3. Receiver operating characteristic curves for the primary 4-sign combined model and individual predictors in the training set (**a**) and validation set (**b**), and comparison of the 4-sign and 5-sign combined models in the training set (**c**) and validation set (**d**). Panels a and b show the primary 4-sign combined model and individual predictors. Panels c and d compare the primary 4-sign model with the 5-sign sensitivity model, including the island sign. Both combined models additionally included irregular hematoma morphology, time from onset to initial CT, male sex, and baseline CT attenuation. The AUC values are shown in the legends. AUC, area under the curve; CT, computed tomography.

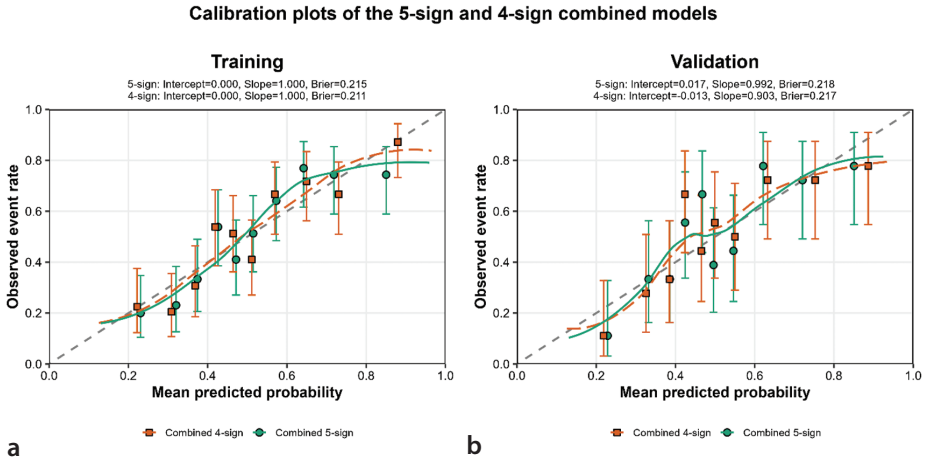

Figure 4. Calibration curves for the primary 4-sign and 5-sign sensitivity models in the training set (**a**) and validation set (**b**). The diagonal dashed line represents perfect calibration. The curves represent the observed relationships between predicted probabilities and actual HE rates for the 4-sign and 5-sign combined models, fitted using locally weighted scatterplot smoothing. Points and error bars show grouped observed event rates and 95% confidence intervals. Calibration intercepts, slopes, and Brier scores are displayed within each panel. HE, hematoma expansion.

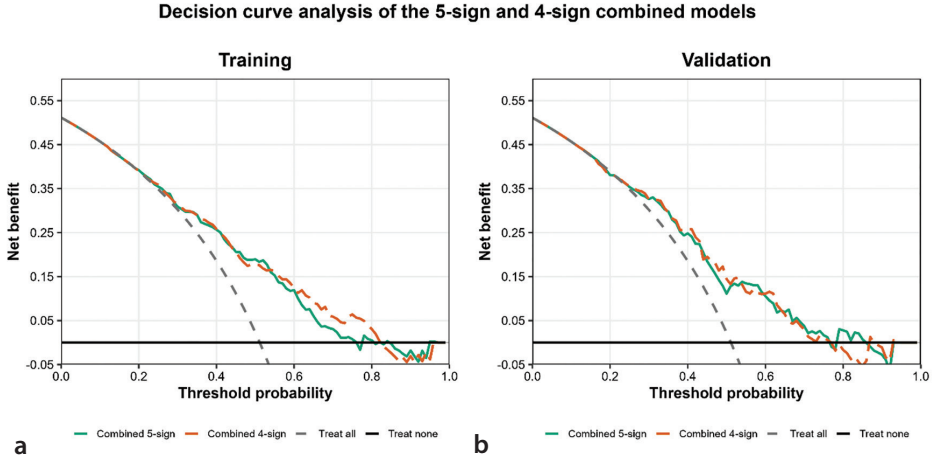

Figure 5. Decision curve analysis of the primary 4-sign and 5-sign sensitivity models in the training set (**a**) and validation set (**b**). Decision curve analysis compares the net benefit of the primary 4-sign combined model and the 5-sign sensitivity model with treat-all and treat-none strategies across a range of threshold probabilities. Both models additionally included irregular hematoma morphology, time from onset to initial computed tomography (CT), male sex, and baseline CT attenuation.

Discussion

ICH accounts for approximately 27.9% of stroke cases globally, and in East Asian populations, it accounts for 18%–24% of all strokes, which is considerably higher than in Western countries.[17,18] Early HE is one of the key mechanisms underlying poor prognosis in ICH. Its reported incidence ranges from 15% to 51%, varying substantially according to the study population and the definition of HE. Once HE occurs, it can lead to further neurological deterioration.[19,20] This study included 571 patients with spontaneous ICH, and the incidence of HE was 51.1%. Based on multivariable logistic regression analysis, the 4-sign comprehensive imaging score, irregular hematoma morphology, time from onset to initial CT, male sex, and baseline CT attenuation were identified as independent factors associated with HE. The primary combined model achieved AUC values of 0.731 and 0.716 in the training and validation sets, respectively. Although this level of discrimination should be interpreted as moderate rather than excellent, the model performed better than any individual variable, suggesting that the integration of multidimensional information may provide additional value for the early identification of HE.

In this study, a comprehensive imaging sign score was constructed by summing the number of positive findings for four NCCT signs: the black hole sign, swirl sign, blend sign, and satellite sign. Multivariate analysis showed that each 1-point increase in this score was associated with an approximately 85% increase in the odds of HE (OR: 1.850, 95% CI: 1.505–2.274, $P < 0.001$). In the training and validation sets, the AUC for this score alone was 0.679 and 0.649, respectively, rendering it the best-performing individual variable in the model. The rationale for this counting approach is that, pathophysiologically, the four included signs are associated with active bleeding and the presence of unclotted or partially clotted blood within the hematoma, reflecting hematoma instability from different perspectives. A previous meta-analysis incorporating 25 studies with a total of 10,650 patients with ICH confirmed that several NCCT markers, including the included signs and the island sign, were associated with HE.[20] Because the island sign was not significantly associated with HE in the present cohort, the primary score was restricted to the four statistically significant signs. A sensitivity analysis that added the island sign produced similar discrimination, calibration, and DCA findings, supporting the robustness of the 4-sign primary model. Previous studies have also suggested that the swirl sign and black hole sign are not only

associated with the risk of HE but also that an increasing number of these signs may correlate with a higher risk of HE.[15,21] Therefore, compared with any single sign, a counting-based comprehensive imaging sign score may better reflect the overall instability of bleeding activity as depicted on NCCT.

Baseline CT attenuation was retained as an independent factor in the multivariate model of this study (OR: 0.964, 95% CI: 0.934–0.995, $P = 0.024$), indicating that lower baseline CT attenuation is associated with a higher risk of HE. Baseline CT attenuation reflects the homogeneity of blood components within the hematoma; regions with low CT attenuation may suggest the coexistence of active bleeding and incompletely coagulated blood, which pathophysiologically corroborates imaging findings such as the swirl sign. Time from onset to initial CT was also retained as an independent factor in the final model (OR: 0.845, 95% CI: 0.750–0.953, $P = 0.006$), suggesting that patients undergoing earlier CT examination are more likely to be in a phase of dynamic HE. Morotti et al.[19] similarly found in a multicenter study that a longer time from onset to imaging was associated with a decreased risk of significant HE. A nomogram study by Yu et al.[22] also incorporated time from onset to initial CT as an independent protective factor. These findings collectively support the important role of the time window factor in early HE identification. In contrast, baseline hematoma volume was significant in univariate analysis but was no longer significant after adjustment. This finding may indicate that, within the multivariable framework, qualitative features of hematoma instability, including irregular morphology and internal density heterogeneity, captured HE-related risk more directly than hematoma size alone. This does not negate the clinical importance of hematoma volume but suggests that volume should be interpreted together with hematoma morphology and density characteristics in early HE assessment.

Irregular hematoma morphology remained an independent factor associated with HE in this study (OR: 2.071, 95% CI: 1.262–3.399, $P = 0.004$). On NCCT, irregular morphology often manifests as lobulated, jagged, or multifocal non-circular contours, potentially indicating simultaneous or sequential bleeding from multiple ruptured vessels, leading to irregular expansion along paths of least resistance. Meta-analyses have confirmed that irregular morphology is significantly associated with both HE and poor functional outcomes.[23] A study related to the Antihypertensive Treatment of Acute Cerebral Hemorrhage II trial also validated this association in a large cohort.[20] Additionally, male sex was retained as an independent factor in this study (OR: 1.500, 95% CI: 1.028–2.189, $P = 0.036$), which is consistent with previous epidemiological studies.[24] This result may be related to differences in blood pressure control, lifestyle, and metabolic risk factors among male patients; however, the underlying mechanisms warrant further investigation. Prior warfarin use was not significantly associated with HE in this cohort. Because only 14 patients had documented prior warfarin exposure, this estimate was imprecise. The retrospective dataset also did not uniformly capture dose, duration, adherence or discontinuation, coagulation status at presentation, or reversal treatment. This finding should therefore not be interpreted as evidence that anticoagulant use is unrelated to HE risk.

The combined model in this study demonstrated higher predictive performance than any individual variable in both the training and validation sets, and calibration curves showed good agreement between predicted probabilities and actual observed probabilities. The AUC values of 0.731 in the training set and 0.716 in the validation set indicate moderate, rather than excellent, discrimination, and the model should not be used as a stand-alone basis for high-stakes treatment decisions. However, DCA showed that the model provided positive net benefit over treat-all and treat-none strategies across a broad range of threshold probabilities in both datasets, suggesting potential practical value as an adjunctive tool for early risk stratification. Compared with previous related studies, the predictive performance of this model was within a comparable range. The 5-sign sensitivity model produced similar discrimination, calibration, and DCA results, supporting the robustness of the more parsimonious 4-sign primary model. Moreover, all variables included in the 4-sign primary model can be obtained from emergency NCCT and routine clinical data, without requiring contrast-enhanced scans or CTA, conferring good practical accessibility.[25] Therefore, for patients with a higher cumulative number of positive imaging signs on admission, irregular hematoma morphology, and a shorter time from onset to initial CT, closer monitoring during the early phase and risk-stratified management may be considered in clinical practice.

Several limitations of this study should be acknowledged. First, this was a single-center retrospective study, which may introduce selection bias and limit generalizability; external validation in other institutional and geographic populations is needed. Second, the NCCT findings were finalized by consensus, and the independent pre-consensus reader assessments were not retained. Therefore, quantitative interobserver agreement, particularly for relatively subjective or uncommon findings such as the island sign, could not be evaluated. Third, hematoma volume was calculated using the Tada formula, which may be less accurate for irregular or lobulated hematomas. Because irregular morphology was independently associated with HE, this limitation should be considered when interpreting the relationships among hematoma shape, estimated volume, and expansion. Fourth, prior warfarin exposure was uncommon, and detailed information on treatment and coagulation status was not uniformly available; the non-significant warfarin result should therefore be interpreted cautiously. Fifth, the relatively high incidence of HE may reflect the characteristics of patients admitted to the participating center. Finally, the definition of HE and the timing of follow-up CT may have influenced outcome determination. Future multicenter prospective studies with standardized imaging assessment, independent reader evaluation, more accurate volumetric methods, and external validation are warranted. In larger cohorts, the incremental value of combining the 4-sign score with additional NCCT markers, including the hematocrit effect, may also be assessed.

Based on NCCT imaging features and clinical data, this study identified five independent factors associated with early HE: a 4-sign comprehensive imaging score, irregular hematoma morphology, time from onset to initial CT, male sex, and baseline CT attenuation. The resulting combined model demonstrated moderate and stable predictive performance in both the training and validation sets, with additional net benefit shown by DCA. All included variables can be obtained directly from emergency NCCT and routine clinical data. These findings suggest that the 4-sign model may serve as a practical adjunct for identifying early HE in patients with ICH.

Footnotes

Conflict of interest disclosure

The authors declared no conflicts of interest.

References

1. Greenberg SM, Ziai WC, Cordonnier C, et al. 2022 guideline for the management of patients with spontaneous intracerebral hemorrhage: a guideline from the American Heart Association/American Stroke Association. *Stroke*. 2022;53(7):e282-e361. [Crossref]
2. Sheth KN. Spontaneous intracerebral hemorrhage. *N Engl J Med*. 2022;387(17):1589-1596. [Crossref] Erratum in: *N Engl J Med*. 2023;388(15):1440. [Crossref]
3. Cordonnier C, Demchuk A, Ziai W, Anderson CS. Intracerebral haemorrhage: current approaches to acute management. *Lancet*. 2018;392(10154):1257-1268. [Crossref] Erratum in: *Lancet*. 2019;393(10170):406. [Crossref]
4. Morotti A, Boulouis G, Dowlatshahi D, et al. Intracerebral haemorrhage expansion: definitions, predictors, and prevention. *Lancet Neurol*. 2023;22(2):159-171. [Crossref]
5. Kase CS, Hanley DF. Intracerebral hemorrhage: advances in emergency care. *Neurol Clin*. 2021;39(2):405-418. [Crossref]
6. Brott T, Broderick J, Kothari R, et al. Early hemorrhage growth in patients with intracerebral hemorrhage. *Stroke*. 1997;28(1):1-5. [Crossref]
7. Dowlatshahi D, Demchuk AM, Flaherty ML, et al. Defining hematoma expansion in intracerebral hemorrhage: relationship with patient outcomes. *Neurology*. 2011;76(14):1238-1244. [Crossref]
8. Wang X, Arima H, Al-Shahi et al. Clinical prediction algorithm (BRAIN) to determine risk of hematoma growth in acute intracerebral hemorrhage. *Stroke*. 2015;46(2):376-381. [Crossref]
9. Al-Shahi Salman R, Frantzias J, Lee RJ, et al. Absolute risk and predictors of the growth of acute spontaneous intracerebral haemorrhage: a systematic review and meta-analysis of individual patient data. *Lancet Neurol*. 2018;17(10):885-894. [Crossref] Erratum in: *Lancet Neurol*. 2018;17(11):933. [Crossref]
10. Morotti A, Dowlatshahi D, Boulouis G, et al. Predicting intracerebral hemorrhage expansion with noncontrast computed tomography: the BAT score. *Stroke*. 2018;49(5):1163-1169. [Crossref] Erratum in: *Stroke*. 2018;49(9):e297. [Crossref]
11. Boulouis G, Morotti A, Brouwers HB, et al. Association between hypodensities detected by computed tomography and hematoma expansion in patients with intracerebral hemorrhage. *JAMA Neurol*. 2016;73(8):961-968. [Crossref]
12. Li Q, Zhang G, Xiong X, et al. Black hole sign: novel imaging marker that predicts hematoma growth in patients with intracerebral hemorrhage. *Stroke*. 2016;47(7):1777-1781. [Crossref]
13. Li Q, Liu QJ, Yang WS, et al. Island sign: an imaging predictor for early hematoma expansion and poor outcome in patients with intracerebral hemorrhage. *Stroke*. 2017;48(11):3019-3025. [Crossref]
14. Yu Z, Zheng J, Ali H, et al. Significance of satellite sign and spot sign in predicting hematoma expansion in spontaneous intracerebral hemorrhage. *Clin Neurol Neurosurg*. 2017;162:67-71. [Crossref]
15. Ng D, Churilov L, Mitchell P, Dowling R, Yan B. The CT swirl sign is associated with hematoma expansion in intracerebral hemorrhage. *AJNR Am J Neuroradiol*. 2018;39(2):232-237. [Crossref]
16. Zhang X, Gao Q, Chen K, et al. A predictive nomogram for intracerebral hematoma expansion based on non-contrast computed tomography and clinical features. *Neuroradiology*. 2022;64(8):1547-1556. [Crossref]
17. GBD 2019 Stroke Collaborators. Global, regional, and national burden of stroke and its risk factors, 1990-2019: a systematic analysis for the Global Burden of Disease Study 2019. *Lancet Neurol*. 2021;20(10):795-820. [Crossref]
18. Lee TH. Intracerebral hemorrhage. *Cerebrovasc Dis Extra*. 2025;15(1):1-8. [Crossref]
19. Morotti A, Li Q, Nawabi J, et al. Predictors of severe intracerebral hemorrhage expansion. *Eur Stroke J*. 2024;9(3):623-629. [Crossref]
20. Morotti A, Boulouis G, Romero JM, et al. Blood pressure reduction and noncontrast CT markers of intracerebral hemorrhage expansion. *Neurology*. 2017;89(6):548-554. [Crossref]
21. Huang L, You Y, He Q, Xie Z. A novel dose-dependent predictor for hematoma expansion on non-contrast CT: the number of black hole signs in spontaneous intracerebral hemorrhage. *Neurosurg Rev*. 2025;49(1):12. [Crossref]
22. Yu F, Yang Y, He Y, et al. Establishment and evaluation of a nomogram model for predicting hematoma expansion in hypertensive intracerebral hemorrhage based on clinical factors and plain CT scan signs. *Ann Palliat Med*. 2021;10(12):12789-12800. [Crossref]
23. Morotti A, Arba F, Boulouis G, Charidimou A. Noncontrast CT markers of intracerebral hemorrhage expansion and poor outcome: a meta-analysis. *Neurology*. 2020;95(14):632-643. [Crossref]
24. Jolink WMT, Wiegertjes K, Rinkel GJE, Algra A, de Leeuw FE, Klijn CJM. Location-specific risk factors for intracerebral hemorrhage: systematic review and meta-analysis. *Neurology*. 2020;95(13):e1807-e1818. [Crossref]
25. Morotti A, Busto G, Boulouis G, et al. Added value of non-contrast CT and CT perfusion markers for prediction of intracerebral hemorrhage expansion and outcome. *Eur Radiol*. 2023;33(1):690-698. [Crossref]